Comprehensive Status Report: November 18, 2004
Project Title: Risk Assessment for Submarine Slope Stability
MMS Project: 491 TO Number: 73648
PI: Steven Wright
COTR: A. Konczvald

This report provides a comprehensive summary of the research completed in the prior Phase of this project (July 2003– August 2004), and describes research being done in the present Phase (September 2004 – August 2005) to complete this project.

Risk Assessment for Submarine Slope Stability: Preliminary Studies and Numerical Modeling of Hydroplaning of Submarine Slides

Stephen G. Wright and Hongrui Hu

1. Introduction

Submarine landslides present an important risk to offshore structures and related facilities. Although submarine slides have many similarities to their subaerial counterparts, there are important differences. As part of previous OTRC research sponsored by the Minerals Management Service Hance (2002) conducted a comprehensive survey and developed an extensive database of submarine slope failures. Hance reported that out of 399 slides reported, 334 occurred on slopes flatter than 10 degree. He also reported that among a total of 434 slides 194 slides traveled a distance greater than 10 km; three slides traveled more than 500 km. The reasons for slides on such flat slopes and with such large travel ("runout") distances are only partially understood. One possible explanation for such large runout distances is that hydroplaning occurs where the slide mass moves on a thin layer of water. There has been some work to explain the movement of a slide mass once hydroplaning is initiated; however, currently there are no tools for predicting how a slope failure that is initiated is transformed into a slide mass that involves hydroplaning.

In the following sections of this report, traditional viscous models of debris flow are first reviewed. Experimental tests and numerical models for hydroplaning are then examined. Next current work pertaining to the pressures and the shear stresses exerted on a debris flow by the surrounding water during hydroplaning is described. Finally, future work pertaining to hydroplaning is discussed.

2. Viscous flow model

Imran et al. (2001) developed a one-dimensional numerical model of muddy subaqueous and subaerial debris flows. In this model, the debris deformation and movement are simulated as an unsteady, nonuniform, laminar slender flow as shown in Figure 1. No flow is assumed to occur in the z direction. The moving mass is assumed to remain continuous, i.e. no one part is assumed to separate from another part. The effect of the surrounding fluid is represented as a simple buoyancy effect; no other stresses are assumed to be imposed on soil by surrounding fluid.

The continuity and equilibrium equations for the coordinate system and slope shown in Figure 1 are as follows:

$$\frac{\partial u}{\partial x}+\frac{\partial v}{\partial y}=0 \tag{1}$$

$$\frac{\partial u}{\partial t}+u\frac{\partial u}{\partial x}+v\frac{\partial u}{\partial y}=-\left(1-\frac{\rho_w}{\rho_d}\right)g\frac{\partial D}{\partial x}+\left(1-\frac{\rho_w}{\rho_d}\right)g\sin\theta+\frac{1}{\rho_d}\frac{\partial \tau_{yx}}{\partial y} \tag{2}$$

$$p=\rho_w g h+\rho_d g(D-y) \tag{3}$$

where u and v are the velocities in the x and y directions, ρ_w and ρ_d are the respective densities of the surrounding water and the debris, g is the acceleration due to gravity, D is the depth of the debris, τ_{xy} is the shear stress on planes parallel and perpendicular to the slope, and h is the depth of the overlying water. The equilibrium equation in the y direction is simplified and reflects a hydrostatic pressure distribution due to the slender flow assumption. Imran et al. used the Herschel-Bulkley rheological model which can be expressed as:

$$\frac{\gamma}{\gamma_r}=\begin{cases}0, & \tau\le\tau_{yield}\\ \left(\dfrac{\tau}{\tau_{yield}}-1\right)^{1/n}, & \tau\ge\tau_{yield}\end{cases} \tag{4}$$

where τ_{yield} is a yield stress and γ_r is a reference strain. This model reduces to a Bingham model when n is 1.0. For this model, the debris can be divided into a shear layer and plug layer. In the plug layer, the velocity is constant along the y direction. The shear layer is the transition between the underlying slope and the overlying plug layer. In the shear layer, the shear stress is larger than the yield stress. The boundary conditions are as follows:

(1) No slip bed at the interface between the debris and slope, i. e. at y = 0,

$$u = v = 0. \tag{5}$$

(2) Kinematic boundary condition at the top of the debris, i.e. at y=D,

$$v=\frac{\partial D}{\partial t}+u\frac{\partial D}{\partial x} \tag{6}$$

Integrating the equation (1) along the y direction gives:

$$\frac{dD}{dt}=-D\frac{\partial \bar{u}}{\partial x} \tag{7}$$

Using the Bingham model and integrating equation (2) within the plug layer and within the whole debris gives:

$$\frac{du_p}{dt}=(\bar{u}-u_p)\frac{\partial u_p}{\partial x}-(\rho_d-\rho_w)g\cos\theta\frac{\partial}{\partial x}(D+D_w)-\frac{\tau_y}{D_p\rho_d}+(\rho_d-\rho_w)g\sin\theta \tag{8}$$

and

$$\frac{d\bar{u}}{dt} = \frac{1}{D}\frac{\partial}{\partial x}\left[\bar{u}^2 D - \frac{1-\alpha_2}{1-\alpha_1}\bar{u}u_p D + \frac{\alpha_1-\alpha_2}{1-\alpha_1}u_p^2 D\right] - (\rho_d - \rho_w)g\cos\theta\frac{\partial D}{\partial x} - \frac{\tau_y}{D\rho_d} + (\rho_d - \rho_w)g\sin\theta \qquad (9)$$

where u_p is the velocity of the plug layer, $\bar{u}$ is the average velocity along the whole depth of mud, τ_y is the yield stress, D_p is the thickness of the plug layer and $\alpha_1 = 2/3$, $\alpha_2 = 8/15$.

For the initial conditions the debris is assumed to be static, consisting of a finite material source and having a given shape. The flow is assumed to stop when the velocity is less than 10cm/s. The one-dimensional system of equations is solved by an explicit finite difference scheme.

Imran et al. validated their model by comparing it with the results from laboratory tests for subaerial slides (Mohrig, et al., 1998). However the model cannot explain why subaqueous debris flows have higher velocities and larger runout distances than subaerial ones even though for subaqueous slides the driving force is reduced by buoyancy and the surrounding water provides increased resistance.

Hance (2003) confirmed the underestimate of runout distances by the viscous flow models. One possible explanation for the large runout distances is hydroplaning. When hydroplaning occurs the debris moves along a thin film of water that is trapped beneath the debris. This thin layer of water behaves as a lubricant and reduces the basal resistance of the debris significantly. The debris can thus move large distances.

3. Experimental tests

Several experimental studies have been conducted that verify the possibility of hydroplaning of debris flows. Mohrig, et al. (1998) performed a series of experiments on debris flows at St. Anthony Falls Laboratory in Minnesota. They conducted the tests in a tank 10 m long, 3 m high and 0.6 m wide. The tank had two segments. The slope of each segment could be varied from 0º (horizontal) to 20º. The slide "debris" was prepared in a concrete mixer with the properties shown in Table 1. Approximately 0.16 m^3 of slurry (debris) was poured at the upper end of the tank in a period of 60 seconds or less. Multiple video cameras were used to track the front of the debris and the distribution of the depth of the debris. Both subaerial and subaqueous slides were modeled by emptying or filling the tank with water.

Mohrig, et al. observed hydroplaning in eight of ten of their subaqueous debris flow experiments. When hydroplaning occurred a wedge of water was observed under the front portion of the debris. A densimetric Froude number defined as follows was proposed to characterize the onset of hydroplaning:

$$Fr_d = \frac{u}{\sqrt{\left(\frac{\rho_d}{\rho_w} - 1\right)gD\cos\theta}} \qquad (10)$$

where u is the average velocity of sliding, ρ_d and ρ_w are the densities of the slurry and water, g is gravity acceleration, D is the average depth of debris and θ is the slope angle of the channel bottom. The minimum value of the Froude number for hydroplaning to occur was reported to be 0.35.

4. Numerical models

Recently two numerical models have been developed to explain hydroplaning of debris flows. The models are based on dynamic lubrication theory. Dynamic lubrication theory and the models for hydroplaning are examined in the following sections.

4.1 Dynamic lubrication theory

Dynamic lubrication theory addresses the two-dimensional flow between two infinitely long flat plates moving relative to each other as shown in Figure 2. The thickness of the gap *h* is assumed to be small. Boundary layer theory is applied and, thus, the kinetic pressure is constant in the *y* direction. There is assumed to be no flow in the *z* direction. The surface forces on an element of fluid are shown in Figure 3. A unit thickness in the *z* direction and a Newtonian liquid are also assumed.

The continuity equation for the fluid can be written as

$$\frac{\partial u}{\partial x}+\frac{\partial v}{\partial y}=0 \tag{11}$$

Flow is fully developed along the x direction, i.e. $\frac{\partial u}{\partial x}=\frac{\partial v}{\partial y}=0$, because $v = 0$ at $y = 0$ and at $y = h$, there is no flow along the y direction. For steady and fully developed flow, the inertial force is zero. Therefore equilibrium of forces on the element in the *x* direction gives:

$$\text{pdy - } \tau \text{ dx - (p+}\frac{\partial p}{\partial x}\text{ dx)dy + } (\tau+\frac{\partial \tau}{\partial y}dy)\,\text{dx} = 0$$

or,

$$\frac{\partial p}{\partial x}-\frac{\partial \tau}{\partial y}=0 \tag{12}$$

where p is pressure and τ is shear stress. The shear stress-strain rate relationship for a Newtonian fluid can be expressed as:

$$\tau=\mu\frac{\partial u}{\partial y} \tag{13}$$

where μ is the dynamic viscosity of the fluid and u is velocity in the x direction. Substituting (13) into (12) gives

$$\frac{\partial p}{\partial x}-\mu\frac{\partial^2 u}{\partial y^2}=0$$

or,

$$\frac{\partial^2 u}{\partial y^2}=\frac{1}{\mu}\frac{\partial p}{\partial x} \tag{14}$$

Next, integrating with respect to *y*:

$$u = \frac{1}{\mu}\left[\frac{1}{2}\frac{dp}{dx}y^2 + c_1(x)y + c_2(x)\right] \tag{15}$$

The following boundary conditions apply:

(1) At $y=0$, $u=0$ (16)

(2) At $y=h(x)$, $u=U$ (17)

where *U* is the relative velocity of the two plates. After substituting the boundary conditions into (15) and determining the constants of integration:

$$u = \frac{1}{2\mu}\left[\frac{dp}{dx}(y^2 - h(x)y)\right] + \frac{U}{h(x)}y \tag{18}$$

Equilibrium of forces in the *y* direction gives:

$$\text{pdx-pdx-}\frac{\partial \text{p}}{\partial \text{y}}\text{dydx-}\tau\text{dy+}\left(\tau+\frac{\partial \tau}{\partial \text{x}}dx\right)\text{dy=0} \tag{19}$$

or, $$\frac{\partial \tau}{\partial x} - \frac{\partial p}{\partial y} = 0 \tag{20}$$

Because p is assumed constant along the y direction, $\partial p/\partial y=0$. Therefore $\partial \tau/\partial x$ must also be zero, i.e. τ is only a function of *y*. Because $\partial u/\partial y$ is equal to τ/μ according to (13), $\partial u/\partial y$ is also only a function of y. Therefore u can be expressed in a form of $u = g(y) + m(x)$, where *g(y)* and *m(x)* are two functions of y and x only. It follows then from Eq. 18 that the thickness, *h*, must be a constant and,

$$u = \frac{1}{2\mu}\left[\frac{dp}{dx}(y^2 - hy)\right] + \frac{U}{h}y \tag{21}$$

Equation (21) shows that the velocity u has a quadratic distribution in the y direction. This characteristic of lubrication theory is applied in the two hydroplaning models described below.

4.2 Gliding block model

Harbitz et al. (2003) developed a one-dimensional analytical solution for steady-state hydroplaning. In their model the slide debris is assumed to be a rigid block moving along a film of water as shown in Figure 4. The slope surface is assumed to be smooth and the slope angle is constant. The flow within the water film is characterized using a modified form of dynamic lubrication theory presented in 4.1. The water film thickness is assumed to change linearly along the block and the distribution of the velocity in the *y* direction is still assumed to be parabolic. The co-ordinate system is fixed relative to the position of the block.

The continuity condition requires:

$$\frac{\partial u}{\partial x}+\frac{\partial v}{\partial y}=0 \tag{22}$$

In the Harbitz et al model the dynamic lubrication theory presented earlier is modified by introducing an additional inertial force in fluid. Equilibrium of forces in the *x* direction then gives:

$$\rho\left(u\frac{\partial u}{\partial x}+v\frac{\partial u}{\partial y}\right)=-\frac{dp}{dx}+\mu\frac{\partial^2 u}{\partial y^2} \tag{23}$$

where *p* is the kinetic pressure and μ is the dynamic viscosity of water.

The boundary conditions are as follows:

(1) At $y = 0$,

$u = -U$ and $v = 0$ (24a)

(2) At $y = h$,

$u = 0$ and $v = 0$ (24b)

(3) At $x = 0$,

$h_{min} = h_T$ and $p = 0$ (24c)

(4) At $x = L$,

$h_{max} = h_L$ and $p=\frac{1}{2}\rho U^2$ (24d)

Based on dynamic lubrication theory, a quadratic distribution of velocity *u* is assumed along the *y* direction:

$$\frac{u}{U}=\left(\frac{y}{h}-1\right)+\frac{h^2}{2\mu U}\frac{dp}{dx}\left(\left(\frac{y}{h}\right)^2-\left(\frac{y}{h}\right)\right) \tag{25}$$

The equations (22), (23) and (25) are then solved analytically with the boundary conditions expressed by equations (24). The solution gives the distributions of velocities and kinetic pressure and shear stress along the bottom of the block. Total forces in directions parallel and perpendicular to the slope and the moment on the block are then calculated by integrating the stresses over the surfaces of the block. The flow rate, Q, across any *x* cross section of the water film is also obtained by integrating *u* along the *y* direction.

The block is assumed to be in equilibrium under a steady state of hydroplaning. The forces and total moment on the block are shown in Figure 5. Kinetic pressure at the front, tail and top surfaces of the block are neglected. Hydrostatic pressure is accounted for by using the submerged weight of the block *G'*. The drag force on the top surface of the block *F3* is estimated using the theory for flow along a flat plate. The normal force, *F1*, on the block is the sum of the kinetic water pressure on the bottom of the block. The shear force, *F2*, on the block is the sum of viscous shear stress

along the bottom of the block. M is the total moment produced by all stresses about the center of the block.

Equilibrium of the block requires that the total forces and total moment to be zero. The three equilibrium equations plus the equation for flow rate (Q) provides four simultaneous nonlinear equations that must be solved for four unknowns. The four unknowns are the block length L, block height H, velocity U and flow rate Q. The variables involved in the solution are summarized in Figure 6 and Table 2.

As part of the current research a series of calculations was performed using Harbitz el al's model. A form of Newton's iterative solution procedure was applied to solve the four simultaneous nonlinear equations numerically. The values of the input parameters are shown in Table 3. A convergence criterion corresponding to a relative error[1] of 10^{-3} was set for the computations. In many cases the iterative solution failed to converge and the solution was not numerically stable. Typical values for the unknowns (L, H, U and Q) are plotted versus the slope angle in Figure 7. Considerable scatter was observed in the computed values, apparently as a result of the error tolerance being too large. Attempts to reduce the apparent scatter by reducing the error tolerance generally failed and the iterations were eventually terminated before convergence was achieved.

In order to determine the potential effect of the kinetic pressures on the moving block Harbitz et al's solution was modified to include a kinetic pressure force on the leading edge of the block. A kinetic pressure equal to the stagnation pressure was assumed to be uniformly distributed along the leading edge of the block. The resulting solutions to the equations with the added kinetic pressure are shown in Figure 8 along with the solutions shown previously in Figure 7. In all cases stable numerical solutions were obtained with relative error of 10^{-8} or smaller.

The ratio of the force, R_p, due to the assumed pressure on the front of the block, to the total resistance R is shown in Figure 9 for the solutions described above. The difference between the forces, R and R_p, is the resistance due to the viscous shear stress along the bottom of the block. As shown in Figure 9(a), the pressure on the front of the block becomes the major source of the resistance as the slope angle increases. For steeper slopes the block is actually physically unstable when the kinetic pressure on the front of the block is neglected. Thus, this appears to be the reason why the numerical solution of Harbitz el al's equations does not converge for steeper slopes. Harbitz et al (2002) considered the block to be essentially infinitely long and, thus, assumed that the front pressure was negligible. This assumption is apparently not valid for many practical situations as shown in Figure 9(b). When the ratio of block length to block height is 10000, the resistance due to the front pressure is still more than 30 percent of the total resistance. Although the front area is much smaller than the bottom area of the block, the resistance due to the front pressure is still important comparing with the basal resistance due to the viscous stress.

The above numerical results based on cursory estimates of the kinetic pressure on the leading edge of the moving block (debris) show the potential importance of such pressures. Unfortunately the actual magnitude and distribution of the kinetic pressures on the block are not well known. Further study of the pressure and stress distribution on the block is necessary. This is discussed further in Section 5.

[1] Relative error is defined as the change in value of any variable on consecutive iterations divided by the value of that variable.

4.3 Modified viscous model

De Blasio, et al. (2004) presented a one-dimensional numerical model for debris flow including possible hydroplaning as shown in Figure 10. This model is essentially an extension of the viscous model developed by Imran et al. (2001) as presented in section 2. This model considers the debris flow as four stages including: (1) the debris flows directly on the ground surface, (2) a wedge of water forms at the interface between the moving debris and underlying ground, (3) the debris hydroplanes and (4) hydroplaning stops and the debris decelerates. It is assumed that hydroplaning only happens when the thickness of the water wedge is a certain size. All the assumptions described for the viscous model in Section 2 still apply and the following additional assumptions are made. When hydroplaning occurs, the kinetic pressure within the water film is assumed to vary linearly along the *x* direction. The distribution of the velocity *u* in the *y* direction is assumed to be parabolic. The resistance forces of the surrounding water on the surfaces of the debris are estimated based on the drag force coefficients derived for the cylinders (Newman, 1977). The kinetic pressure on the top surface of the debris is neglected.

A reference coordinate system that is fixed relative to the stationary slope is used as shown in Figure 10. The continuity and equilibrium equations in the *x* and *y* directions for both mud and water have the same form as follows:

$$\frac{\partial u}{\partial x}+\frac{\partial v}{\partial y}=0 \tag{26}$$

$$\frac{\partial u}{\partial t}+u\frac{\partial u}{\partial x}+v\frac{\partial u}{\partial y}=\frac{1}{\rho}\left(-\frac{\partial p}{\partial x}+\frac{\partial \tau_{yx}}{\partial y}\right)+g\sin\theta \tag{27}$$

$$-\frac{1}{\rho}\frac{\partial p}{\partial y}-g\cos\theta=0 \tag{28}$$

where ρ is the density of the medium (either ρ_d or ρ_w for mud or water, respectively), p is the pressure, τ_{xy} is the shear stress on the *y* plane along the *x* direction and *g* is the acceleration due to gravity. The equilibrium equation in the *y* direction has been simplified using the slender flow assumption used in the viscous flow model presented previously in Section 2.

The boundary conditions for the water and mud are as follows:

(1) At the ground surface i.e. *y=0*,

$$u=v=0 \tag{29}$$

(2) At the top of the debris ($y = D + D_w$),

$$v=\frac{\partial(D+D_w)}{\partial t}+u\frac{\partial(D+D_w)}{\partial x} \tag{30}$$

(3) At the top of the water layer ($y = D_w$),

$$v=\frac{\partial D_w}{\partial t}+u\frac{\partial D_w}{\partial x} \tag{31}$$

(4) At the interface between the debris and water ($y = D_w$),

$$\tau_{xy}\Big|_{debris} = \tau_{xy}\Big|_{water} \tag{32}$$

where D is the depth of the debris and D_w is the thickness of the water film (D_w is zero when there is no water trapped beneath the debris). Equations (29) and (30) apply for all flow of the debris, while Equations (31) and (32) only apply while water is trapped under the debris.

The debris flow is modeled in four stages. Stage one is at the beginning of the debris flow. There is no water underneath the mud, i.e. D_w is zero. Integrating Equations (26), (27) and (28) along the y direction over the depth of the debris gives:

$$\frac{dD}{dt} = -D\frac{\partial \bar{u}}{\partial x} \tag{33}$$

$$\frac{du_p}{dt} = (\bar{u} - u_p)\frac{\partial u_p}{\partial x} - (\rho_d - \rho_w)g\cos\theta\frac{\partial}{\partial x}(D + D_w) - \frac{\tau_t + \tau_y}{D_p\rho_d} + (\rho_d - \rho_w)g\sin\theta \tag{34}$$

$$\frac{d\bar{u}}{dt} = \frac{1}{D}\frac{\partial}{\partial x}\left[\bar{u}^2 D - \frac{1-\alpha_2}{1-\alpha_1}\bar{u}u_p D + \frac{\alpha_1 - \alpha_2}{1-\alpha_1}u_p^2 D\right]$$

$$-(\rho_d - \rho_w)g\cos\theta\frac{\partial D}{\partial x} - \frac{\tau_b + \tau_y}{D\rho_d} + (\rho_d - \rho_w)g\sin\theta \tag{35}$$

$$\tau_t = -\frac{1}{2}\rho_w C_F u_p^2 \tag{36}$$

$$\alpha_1 = 2/3 \tag{37}$$

$$\alpha_2 = 8/15 \tag{38}$$

$$\tau_b = sign(u_p)\tau_y\left[1 + \left|2\frac{u_p}{D_s\gamma_r}\right|\right] \tag{39}$$

In the above equations, u_p is the velocity of the plug layer where the velocity u is constant, $\bar{u}$ is the average velocity along the whole depth of mud including the plug layer and the shear layer, D_p is the thickness of the plug layer, τ_t is the shear stress at the top of the mud. The shear stress, τ_y, is the yield stress of the mud and τ_b is the shear stress at the bottom of the mud. D_s is the thickness of the shear layer and C_F is the drag force coefficient. These equations apply when the debris is in direct contact with the ground surface and reduce to those of the viscous flow model when τ_t is zero.

The second stage of flow ("Stage Two") starts when the velocity of the plug layer reaches a "critical" value. At this point a wedge of water is introduced suddenly at the interface between the debris and the ground surface near the front of the debris flow. The shape of the wedge is assumed as arbitrary input quantity. The critical velocity where the wedge of water is introduced is related to a "critical" Froude number defined as:

$$Fr_{crit} = \sqrt{\frac{\rho_w \overline{u}^2}{g \cos\theta (\rho_d - \rho_w) D}} \tag{40}$$

The value of the critical Froude number is selected arbitrarily as 1.0. At the point where the wedge of water is introduced Equations (33) to (39) still apply in the debris. For the water wedge, Equations (26), (27) and (28) are integrated along the *y* direction within the wedge to give:

$$\frac{dD_w}{dt} = \overline{u}\frac{\partial D_w}{\partial x} - \frac{\partial f_w}{\partial x} \tag{41}$$

$$\frac{df_w}{dt} = \left(\frac{6}{5}\overline{u} - \frac{12}{5}\frac{f_w}{D_w}\right)\frac{\partial f_w}{\partial x} + \left(\frac{6}{5}\left(\frac{f_w}{D_w}\right)^2 - \frac{2}{15}\overline{u}^2\right)\frac{\partial D_w}{\partial x}$$

$$-\left(-\frac{1}{5}f_w + \frac{4}{15}\overline{u}D_w\right)\frac{\partial \overline{u}}{\partial x} - \frac{\rho_d - \rho_w}{\rho_w} g\cos\theta D_w \frac{\partial D}{\partial x} + \frac{\mu_w}{\rho_w}\left(6\frac{\overline{u}}{D_w} - 12\frac{f_w}{D_w^2}\right) \tag{42}$$

where f_w is the flow rate within the water wedge and μ_w is the dynamic viscosity of water.

The third stage of flow ("Stage Three") is the stage where the debris hydroplanes. When D_w is larger than the height of the roughness at the interface between the debris and the underlying slope, hydroplaning is assumed to start. De Blasio et al. assumed that the height of the roughness was several millimeters in the laboratory tests and several decimeters for field cases. When hydroplaning occurs Equations (41) and (42) still apply in the water beneath the moving debris. The debris is assumed to move as a plug with a uniform velocity u_p throughout equal to $\overline{u}$. Integrating equations (26), (27) and (28) along the *y* direction within the debris gives:

$$\frac{dD}{dt} = -D\frac{\partial \overline{u}}{\partial x} \tag{43}$$

$$\frac{d\overline{u}}{dt} = -(\rho_d - \rho_w) g\cos\theta \frac{\partial (D + D_w)}{\partial x} - \frac{\tau_t + \tau_w}{D\rho_d} + (\rho_d - \rho_w) g\sin\theta + f_p \tag{44}$$

$$f_p = -\frac{1}{2}\frac{\rho_w}{\rho_d}\frac{C_P}{D}\left|\frac{\partial D}{\partial x}\right| u_p^2 \tag{45}$$

where C_P is the pressure drag coefficient.

"Stage Four" is the stage after hydroplaning ceases. It is assumed that when D_w reaches a value that is smaller than the assumed height of the roughness, the debris flow reverts to "Stage Two" flow and the debris decelerates until it stops.

The modified viscous model described above has several limitations due to the following:

1. The "critical" Froude number that marks the stage where the water wedge is introduced is assumed.
2. The initial shape of the water wedge is assumed.
3. The height of the roughness at the interface of the debris and the underlying slope is assumed.
4. The drag forces exerted on the debris by the surrounding fluid are estimated based on drag coefficients developed for an object with a totally different shape (a cylinder). Significant differences in drag forces are anticipated for objects with different shapes.

Further studies are needed to define better the distributions of kinetic pressure and shear stress on the surfaces of the moving debris as well as the development of the water wedge (initial onset of hydroplaning). Both require developing a better understanding of the flow around the debris and within any "wedge" of water that forms beneath the front of the debris. This is discussed in Section 5.

4.4 Modeling of pneumatic tire hydroplaning

Another approach for modeling hydroplaning of debris is to model the debris as a deformable solid body, somewhat like what has been done for hydroplaning of pneumatic vehicle tires. In this case the stress in the hydroplaning body is related to the deformation and strain in the body.

Browne and Whicker (1983) developed a model for tire-fluid interaction during steady-state hydroplaning of a tire. They modeled the deformable and possibly rotating tire coupled with the flow in the water film between the tire and underlying pavement. The pavement was assumed to be a rigid smooth semi-infinite half-space. The tire was assumed to deform under a total load from an axle with differential inner and outer tire pressures. The physical model is illustrated schematically in Figure 11. The framework of Browne and Whicker's model is described briefly in the following paragraph; however, detailed information about the analysis is omitted.

In Browne and Whicker's model the total system is decoupled into tire and fluid flow subsystems. The deformation of the tire is modeled using the finite element method. For this analysis the tire is assumed to be an elastic body. The flow at the interface of the tire and the pavement is modeled by the "control volume" method. For this the tire and the pavement are assumed to be rigid bodies. The compatibility conditions between the two subsystems are: (1) the deformed shape of the tire and the shape of the water film at the contact are the same, and (2) the outer pressure and shear stress on the tire equal to the corresponding stresses in the adjacent fluid. An iterative procedure is used to achieve the compatibility between the two subsystems (tire and fluid). A flow chart of the steps in the tire hydroplaning model is shown in Figure 12. Two levels of iteration and convergence are required for the compatibility as follows:

1. Starting with a trial axle height, the tire compliance matrix for the finite element model is constructed using the elastic properties and the initial geometry of the tire. Next an initial distribution of the thickness of the water film is assumed, and the fluid flow analysis is conducted. A kinetic pressure is determined from the flow analysis. This

pressure is used to calculate (update) the deformation in the tire using the finite element method again. If the deformation of the tire is compatible with the shape of the water film, the first level of convergence is achieved. If not, a new distribution of the thickness of the water film is assumed according to the deformation of the tire, and the analyses for the tire and the flow are repeated. These two analyses are performed iteratively until the first level of convergence is reached.

2. Once the first level of convergence is achieved the pressures at the top surface of the water film are integrated to obtain the total force on the tire. If the total force balances the axle load on the tire, equilibrium is satisfied, i. e. the second level of convergence and final solution are attained. If instead the total load does not equal the axle load, the assumed axle height is changed and all the analyses presented above are repeated until the second level of convergence is reached. Once the second level of convergence is achieved the thickness of the water film, the kinetic pressure and the axle height are known for the selected load and tire velocity.

By adopting an approach like the one described above to analyze hydroplaning of debris flows the soil body could be treated as a deformable solid sliding on a film of water. Treating the soil as a deformable solid may be a more realistic approach than treating the soil as a visco-plastic material. With such an approach the motion of the debris could be modeled by analyzing the total force on the debris, including the force due to its self-weight and forces exerted by the surrounding fluid. However, unlike a tire, which may be treated as an elastic solid, the debris should probably be treated as an inelastic or elasto-plastic solid.

5. Flow around a gliding block

Mohrig, et al. (1998) found that the critical Froude number for the onset of hydroplaning is 0.35. Based on the definition of the Froude number (Equation 10) it can be shown that a Froude number of 0.35 corresponds to a kinetic pressure that is only 6.1 percent of the stress due to the buoyant weight of the debris. This suggests that the debris hydroplanes when the effective stress at the bottom of the debris is still significantly larger than zero. This apparent discrepancy may result from neglecting negative kinetic pressures on the top surface of the debris. Also, the results and discussion presented earlier in Section 4.2 suggest the importance of the pressures on the front of the moving debris. De Blasio, et al. (2004) estimated the kinetic pressure and shear stress on all the surfaces of the debris based on drag coefficients that may not be correct. All this suggests that further study of the pressures and shear stresses on the surfaces of the debris is warranted. Also, the numerical models assume the applicability of boundary layer theory and a parabolic distribution of velocity within the water film. The validity of these assumptions on the flow within the water film also needs to be examined.

In order to examine the validity of the various assumptions and approximations about the flow around the debris as described in earlier studies, analyses of the flow around debris have been initiated as part of the current research. A numerical model has been developed for the interaction of debris and ambient fluid. The model is illustrated schematically in Figure 13. Several assumptions are made including:

1. the debris body is a rigid block.
2. the ground surface is smooth.
3. the fluid is water with constant physical properties.

4. the thickness of the water film is constant.
5. the flow is two-dimensional, incompressible, steady and laminar.

The coordinate system is assumed to move with the block. Because the flow is steady and the block slides with a constant velocity U relative to the surrounding fluid and underlying solid surface, the coordinate system is an inertial reference system. In the coordinate system the block is stationary, and the incoming fluid and underlying ground surface have a constant, reference velocity U. At the left side of the domain a fully developed flow boundary condition is assumed. The commercial software, Fluent 5/6, is used to solve the problem numerically. Fluent is a computational fluid dynamics code employing a finite volume scheme. The commercial preprocessing software, Gambit, is used to discretize the flow domain. Meshes consist of boundary layer elements and structured elements around the block; some unstructured elements are used for transitions between structured elements.

The numerical model solves the continuity and equilibrium equations in the x and y directions, which are as follows:

$$\frac{\partial u}{\partial x}+\frac{\partial v}{\partial y}=0 \tag{46}$$

$$\frac{\partial u}{\partial t}+u\frac{\partial u}{\partial x}+v\frac{\partial u}{\partial y}=\frac{1}{\rho_w}\left(-\frac{\partial p}{\partial x}+\frac{\partial \tau_{yx}}{\partial y}+\frac{\partial \sigma_{xx}}{\partial x}\right) \tag{47}$$

$$\frac{\partial v}{\partial t}+u\frac{\partial v}{\partial x}+v\frac{\partial v}{\partial y}=\frac{1}{\rho_w}\left(-\frac{\partial p}{\partial y}+\frac{\partial \tau_{yx}}{\partial x}+\frac{\partial \sigma_{yy}}{\partial y}\right) \tag{48}$$

where ρ_w is the density of water, p is the kinetic pressure, σ_{xx} and σ_{yy} are the normal stresses and τ_{xy} is the shear stress. The gravity force and the hydrostatic pressure are not included in the equations (47) and (48) because their influences on the flow cancel each other. The boundary conditions are as follows:

(1) At the far right side of the region ($x=L_t$),

$$u = -U,\ v=0 \tag{49}$$

(2) At the far left side of the region ($x=0$),

$$\frac{\partial u}{\partial x}=\frac{\partial v}{\partial x}=0 \tag{50}$$

(3) At the bottom surface ($y = 0$),

$$u = -U,\ v=0 \tag{51}$$

(4) At the top of the region ($y=H_t$),

$$u = -U,\ v=0 \tag{52}$$

(5) At the bottom of the rigid block ($y = h$ and $X_0 < x < X_0 + L$),

$$u = 0,\ v=0 \tag{53}$$

(6) At the top of the rigid block ($y = H + h$ and $X_0 < x < X_0 + L$),

$$u = 0,\ v=0 \tag{54}$$

(7) At the left side of the block ($x = X_0$ and $h < y < H + h$),

$$u = 0,\ v=0 \tag{55}$$

(8) At the right side of the block ($x = X_0 + L$ and $h < y < H + h$),

$$u = 0,\ v=0 \tag{56}$$

Work is currently being done using the model described above to study the flow around a moving mass during hydroplaning. Sensitivity issues related to mesh size and configuration have been investigated. Significant numerical problems are still being encountered with residual errors exceeding what are believed to be acceptable limits. Most of the numerical problems are believed to be a result of flow separation around the sharp corners of the block. Work is currently in progress to smooth the corners of the block and to minimize effects of flow separation.

6. Discussion and future work

Hydroplaning of submarine slides occurs when a thin layer of fluid forms at the interface between the moving slide debris and the underlying ground surface. The layer of water acts as a "lubricant" and decreases the shear resistance on the debris exerted by the underlying ground. Hydroplaning occurs when the effective normal stress between the debris and underlying slope becomes zero. As the sliding velocity of the debris increases, the total kinetic pressure force on the debris increases. When this pressure force balances the component of the submerged soil weight in the direction normal to the slope, fluid penetrates beneath the debris and hydroplaning is initiated. Based on a review of previous research as well as the discussion and work described in the previous sections of this report, the following characteristics of hydroplaning are found:

1) Hydroplaning increases the run-out distance and sliding velocity of the debris and decreases the thickness of the final debris deposit.
2) Hydroplaning is related to the hydrodynamic conditions of the flow including the velocity and the kinetic pressure. It is different from the simple reduction of the basal friction due to the wetting of the sediment.
3) Hydroplaning is more likely to occur in slide debris that is rich in clay because dissipation of trapped water due to infiltration into the soil is negligible.
4) Hydroplaning is independent of the rheological properties of the debris.
5) The front of the debris becomes blunter when hydroplaning happens.
6) Attenuation right behind the blunt front and even autoacephalation (complete detach of head from the main debris body) occur when hydroplaning happens.
7) Hydroplaning decreases the remobilization of the bed soil and the mass entrainment into the debris from the bed soil during the sliding.

8) The cessation condition of hydroplaning can be the change of the slope of the bed, the dissipation of the fluid trapped underneath the debris, the increase of the roughness of the bed surface or the soil shedding from the debris into the surrounding fluid.

Until now, almost all research pertaining to hydroplaning of slide debris has been limited within the stage of the debris flow. The transition from the failed slope, i. e. once a slide is initiated to a moving slide mass is not well understood. Accordingly future work will include:

1) Continuing study of the pressure and shear stress on the surfaces of the moving slide mass applied by the surrounding flow using numerical modeling and similitude analysis;
2) Study of the initiation mechanisms of the slope failure including the increase of the driving load and the reduction of the soil resistance;
3) Development of an analytical/numerical model for debris flow including the initiation of the slope failure, the transition between the failed slope and the debris flow, the moving debris, including possible hydroplaning, and the final deposition of the debris following movement;
4) Verification of the model with realistic laboratory experiments and available field data.

Reference

De Blasio, F. V., Engvik, L., Harbitz, C. B. and Elverhøi, A., (2004),"Hydroplaning and submarine debris flows," *Journal of geophysical research*, Vol. 109, C01002, doi: 10.1029/2002JC001714.

Browne, A. L. and Whicker, D., (1983), "An interactive tire-fluid model for dynamic hydroplaning," *Frictional interaction of tire and pavement*, *ASTM STP 793*, Meyer, W. E. and Walter, J. D., Eds., American society for testing and materials, pp. 130-150.

Hance, J. J., (2003), "Development of a database and assessment of seafloor slope stability based on published literature," M.S. thesis, the university of Texas at Austin.

Harbitz, C.B., Parker, G., ElverhΦi, A., Marr, J.G., Mohrig, D., and Harff, P.A., 2003, "Hydroplaning of subaqueous debris flows and glide blocks: Analytical solutions and discussion," *Journal of Geophysical Research*, 108(B7), 2349, doi:10. 1029/2001 JB001454.

Imran, J., and Parker, G.,. (2001), "A numerical model of muddy subaqueous and subaerial debris flows," *Journal of hydrodynamic engineering*, Vol. 127, Issue 11, pp. 959-968.

Juvinall, R.C., 1983, *Fundamentals of machine component design*, John Wiley & Sons, pp. 399-402.

Mohrig, D., Ehipple, K. X., Hondzo, M. Ellis, C. and Parker, G, 1998, Hydroplaning of subaqueous debris flows, *Geological Society of America Bulletin*, 110, pp 387-394.

Newman, J.N., (1977), *Marine Hydrodynamics*, 415, pp., MIT press, Cambridge, Mass.

Reynold, O., 1886, "On the theory of lubrication and its applications to Mr. Beauchamp Tower's experiments," *Philosophical Transactions of the Royal Society* (London), 177, pp. 157-234.

White, F. M., 1979, *Fluid mechanics*, McGraw-Hill, Inc., pp. 95-96.

Table 1. Properties of the debris soil used in the experiments by Mohrig et al. (1998)

Properties		Note
Water content	16.5%	
Bulk density	2.08 (±0.03) × 10^3 kg/m^3	
D_{50}	57 μm	
Mineralogy	Quartz only	
Hydraulic conductivity	3 × 10^{-5} m/s	Estimated according to grain size distribution
Yield strength	29 Pa	Estimated by complementary studies of half-pipe channel flows
Viscosity	14 Pa-s	

Table2. Definition of symbols

Symbol	Definition
L	Block length (m)
H	Block height (m)
U	Velocity of block relative to slope (m/s)
θ	Slope angle (degree)
Q	Flow rate per unit width across any x cross-section of the water film (m^2/s)
h_T	Thickness of the water film at the tail (m)
h_L	Thickness of the water film at the front (m)
q	$Q/(Uh_T)$
k	h_T/L
r	h_L/h_T (>1)
ν_w	Kinematic viscosity of the surrounding fluid (m^2/s)
R_s	Submerged specific gravity of the sliding block $\left(\frac{\rho_{block}}{\rho_w}-1\right)$
ς	Relative viscosity of water film to surrounding fluid $\left(\frac{\nu_s}{\nu_w}\right)$
Fr	Densimetric Froude number $\frac{U}{\sqrt{R_s g H}}$
h	$\frac{h_T + h_L}{2}$
Re	Renolds number $\frac{Uh}{\nu_s}$
Relative error	Maximum of $\frac{dx_i}{x_i}$, $i=1, 2, 3$ and 4. x_i are H, L, U and q.

Table 3. Values of the input parameters used for computations with gliding block model

ν_w (m^2/s)	r	k	θ (degree)	R_s	ς
1.00E-06	4	5.00E-05	Varies (10^{-3} to 10)	0.8	1.0

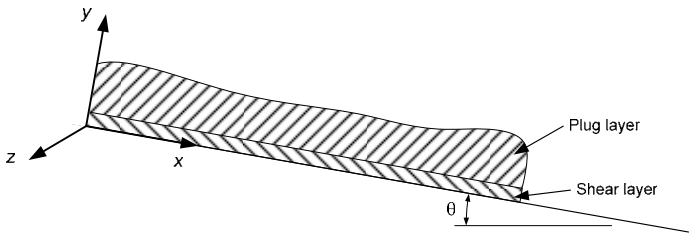

Figure 1 – Viscous flow model of landslide.

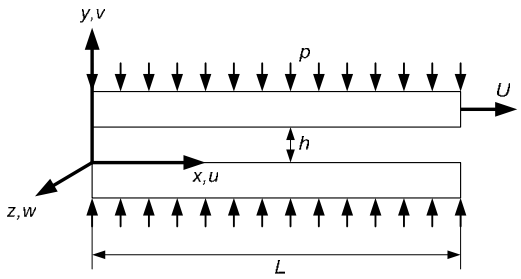

Figure 2 – Fluid film between two parallel, flat plates.

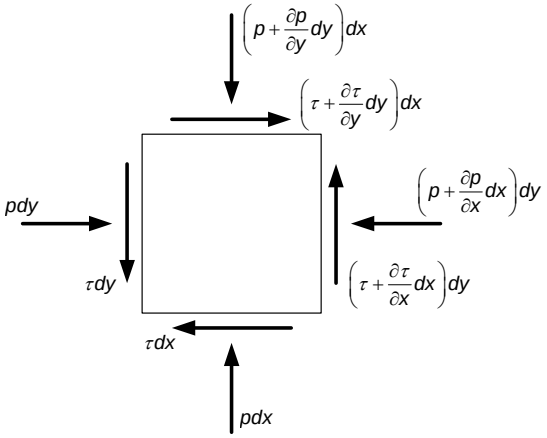

Figure 3 – Forces on an element of fluid,

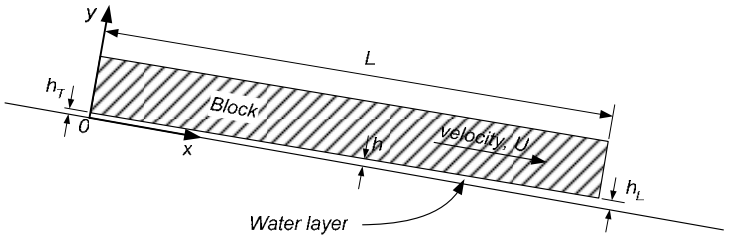

Figure 4 – Sliding block on a slope with stable hydroplaning.

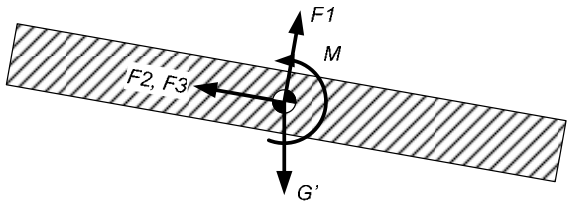

Figure 5 – Forces and moments on a rigid block during hydroplaning.

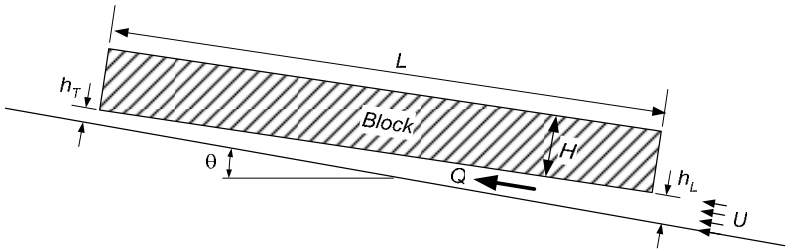

Figure 6 – Variables for the gliding block model.

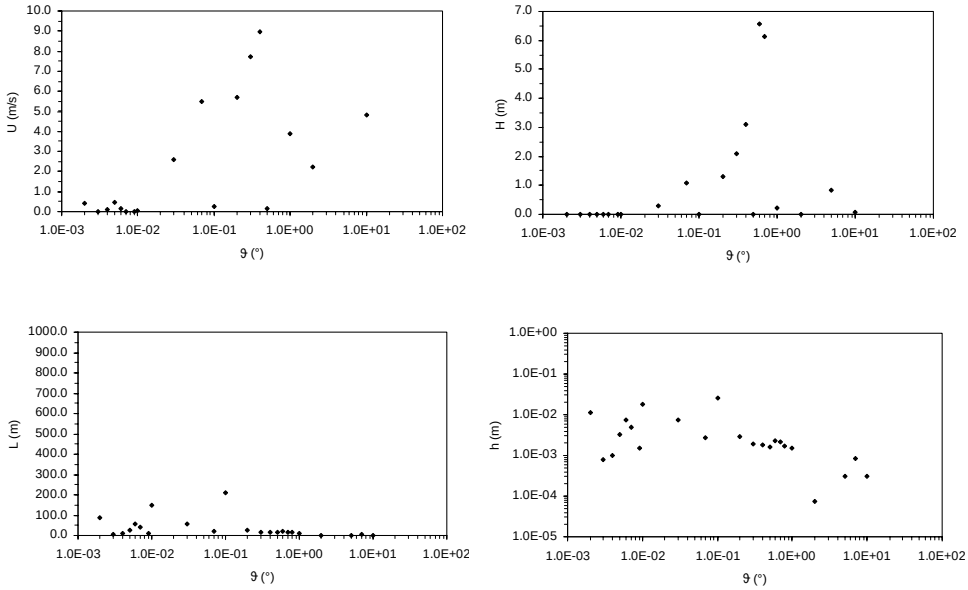

Figure 7 – Calculated values using Harbitz et al. model (unmodified).

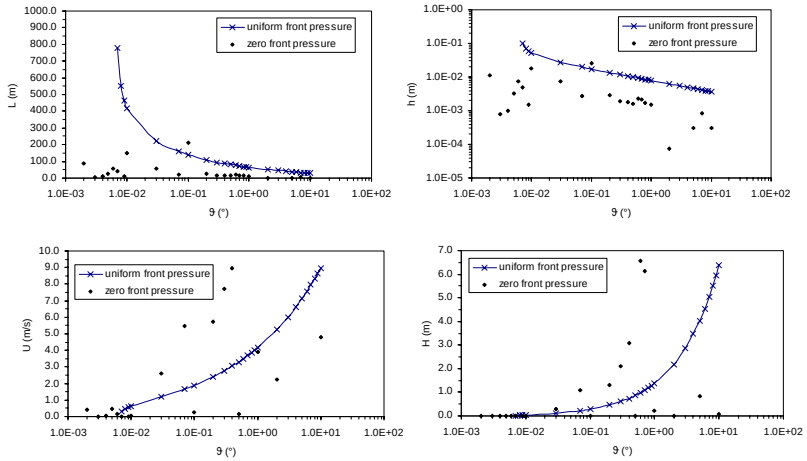

Figure 8 – Calculated values using Harbitz el al. model with and without modification for pressure force on leading edge of sliding block.

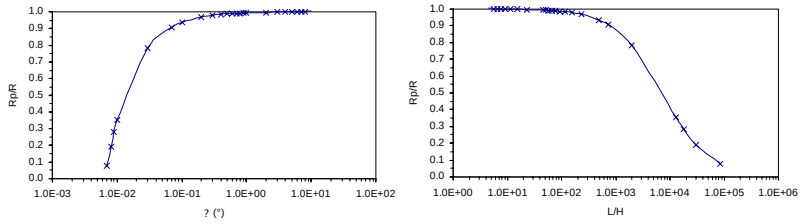

(a) (b)

Figure 9 – Variation with slope angle of the relative resistance defined as the ratio of force due to pressure on the leading edge to the total resisting force.

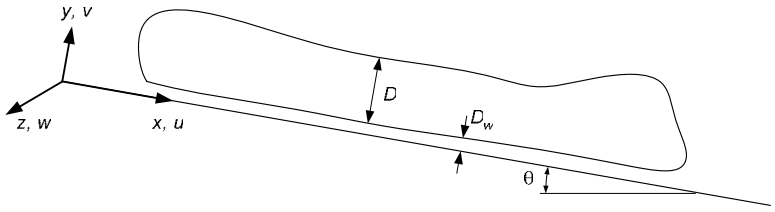

Figure 10 – Modified viscous flow model.

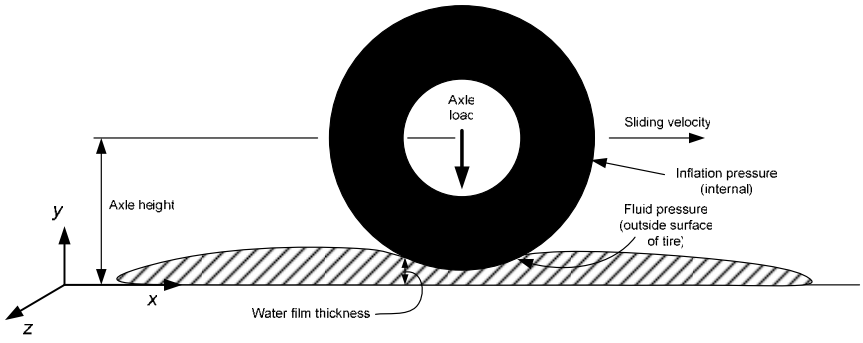

Figure 11 – Hydroplaning model for a pneumatic tire.

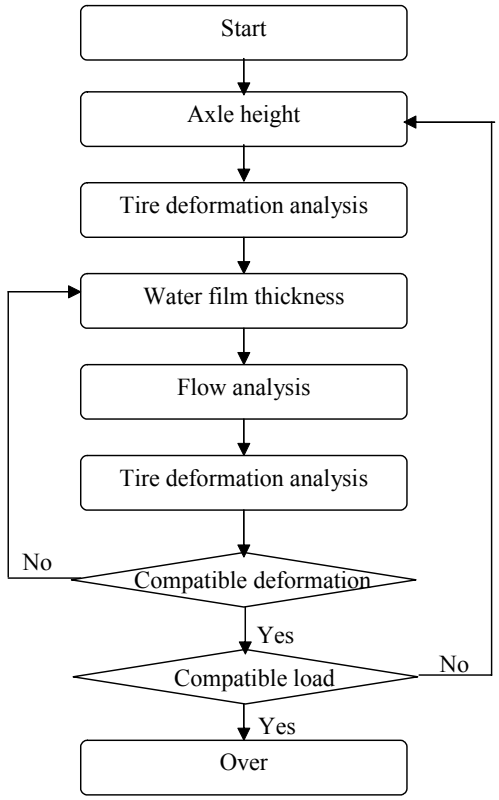

Figure 12 - Flow chart for the pneumatic time hydroplaning model

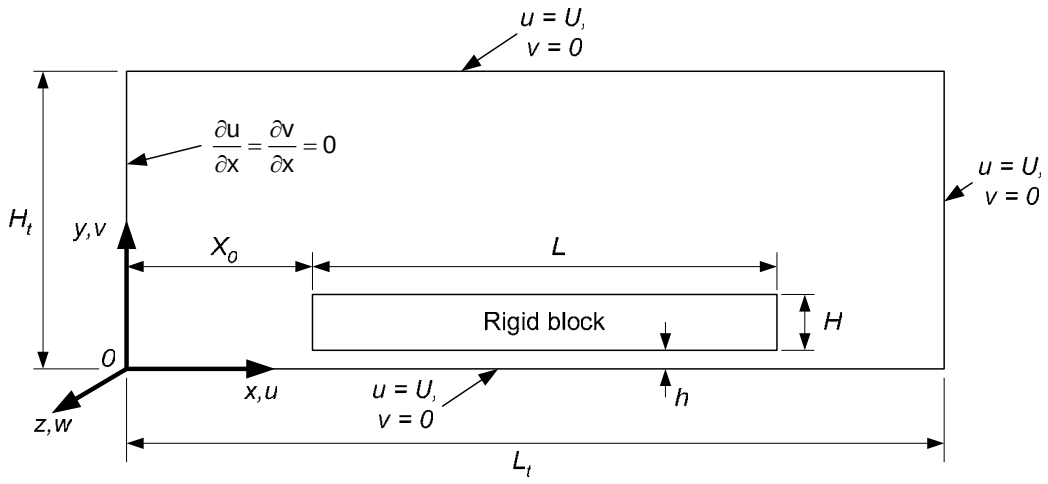

Figure 13 – Flow around a sliding block.